LETTER

doi:10.1038/nature20611

Identification of an atypical monocyte and committed progenitor involved in fibrosis

Takashi Satoh[1,2]*, Katsuhiro Nakagawa[1,2]*, Fuminori Sugihara[3], Ryusuke Kuwahara[4], Motooki Ashihara[5], Fumihiro Yamane[1,2], Yosuke Minowa[5], Kiyoharu Fukushima[1,2], Isao Ebina[1,2,5], Yoshichika Yoshioka[3], Atsushi Kumanogoh[6,7] & Shizuo Akira[1,2]

Monocytes and macrophages comprise a variety of subsets with diverse functions[1–5]. It is thought that these cells play a crucial role in homeostasis of peripheral organs, key immunological processes and development of various diseases. Among these diseases, fibrosis is a life-threatening disease of unknown aetiology. Its pathogenesis is poorly understood, and there are few effective therapies. The development of fibrosis is associated with activation of monocytes and macrophages[6–8]. However, the specific subtypes of monocytes and macrophages that are involved in fibrosis have not yet been identified. Here we show that Ceacam1$^+$Msr1$^+$Ly6C$^-$F4/80$^-$Mac1$^+$ monocytes, which we term segregated-nucleus-containing atypical monocytes (SatM), share granulocyte characteristics, are regulated by CCAAT/enhancer binding protein β (C/EBPβ), and are critical for fibrosis. *Cebpb* deficiency results in a complete lack of SatM. Furthermore, the development of bleomycin-induced fibrosis, but not inflammation, was prevented in chimaeric mice with *Cebpb*$^{-/-}$ haematopoietic cells. Adoptive transfer of SatM into *Cebpb*$^{-/-}$ mice resulted in fibrosis. Notably, SatM are derived from Ly6C$^-$FcεRI$^+$ granulocyte/macrophage progenitors, and a newly identified SatM progenitor downstream of Ly6C$^-$FcεRI$^+$ granulocyte/macrophage progenitors, but not from macrophage/dendritic-cell progenitors. Our results show that SatM are critical for fibrosis and that C/EBPβ licenses differentiation of SatM from their committed progenitor.

To identify fibrosis-related monocyte/macrophage subsets, we first investigated which subsets are increased only in the fibrotic phase. Although multiple cell types are included both in Ly6C$^+$ and Ly6C$^-$ populations, detailed classification of the respective cell types has yet to be fully performed[9]. Although Ly6C$^+$ inflammatory monocytes and Ly6C^{dull} neutrophils were both increased in the inflammatory phase, Ly6C$^-$Mac1$^+$ cells were markedly increased in the fibrotic phase (Fig. 1a, b). Fluorescence-activated cell sorting (FACS) analysis of the Ly6C$^-$Mac1$^+$ subset showed that three major populations were present (Fig. 1c). Comprehensive gene expression analysis clearly indicated that the expression pattern of each monocyte was completely different (Fig. 1d, e, Extended Data Fig. 1a). Of these cell types, adoptive transfer of only Ceacam1$^+$Msr1$^+$Ly6C$^-$F4/80$^-$Mac1$^+$ monocytes into bleomycin-treated wild-type mice led to exacerbation of fibrosis (Fig. 1f, Extended Data Fig. 1b, c). As these cells highly expressed C/EBPβ (Fig. 1d, g), we examined whether this molecule in haematopoietic cells contributes to fibrosis. Chimaeric mice with *Cebpb*$^{-/-}$ haematopoietic cells showed marked resistance to fibrosis with low hydroxyproline content, no elevation of mRNA involved in fibrosis and no fibrotic area by magnetic resonance imaging (MRI), but underwent normal inflammation (day 4 after treatment) accompanied by body weight reduction, accumulation of inflammatory cells and induction of mRNA and proteins involved in inflammation (Fig. 1h–l, Extended Data Fig. 2a–f; Supplementary Videos S1–S5). By contrast, *Cebpd*$^{-/-}$ mice did not show any defects in development of fibrosis (Extended Data Fig. 3a, b). Furthermore, a modified high-fat diet liver fibrosis model also clearly showed that fibrosis was suppressed in *Cebpb*$^{-/-}$ chimaeras (Extended Data Fig. 4a–c). However, wound healing progressed normally (Extended Data Fig. 5a–c). These findings indicate that fibrosis, but not inflammation, was prevented in *Cebpb*$^{-/-}$ chimaeras.

Whereas the proportions of almost all immune cells were normal, Ceacam1$^+$Msr1$^+$Ly6C$^-$F4/80$^-$Mac1$^+$ monocytes were completely absent in *Cebpb*$^{-/-}$ chimaeras (Fig. 2a, Extended Data Fig. 6a, b). These monocytes had a bi-lobed segmented nuclear shape and many cytoplasmic granules (Fig. 2b and Supplementary Video S6). Thus, these cells were termed segregated-nucleus-containing atypical monocytes (SatM) on the basis of this unique nuclear shape and hybrid characteristics of both monocytes and granulocytes as described below. Moreover, the *Cebpb*$^{-/-}$ chimaeras reconstituted with SatM developed fibrosis (Fig. 2c–e, Extended Data Fig. 2g). Retrovirally expressed C/EBPβ in *Cebpb*$^{-/-}$ bone marrow was sufficient to restore SatM differentiation (Fig. 2f, g).

Numerous studies have shown that transforming growth factor (TGF)-β is an essential factor for fibrosis. Interestingly, TGF-β production in the lung was significantly impaired in *Cebpb*$^{-/-}$ chimaeras after bleomycin administration (Fig. 2h). However, SatM did not express TGF-β (Extended Data Fig. 7a), indicating that repressed TGF-β production in *Cebpb*$^{-/-}$ chimaeras is indirectly influenced by the loss of SatM. Given that Spp1 is an initiation factor for fibrosis[10], we investigated expression of Spp1 at the beginning of fibrosis. *Spp1* mRNA in the lung was markedly decreased in bleomycin-treated *Cebpb*$^{-/-}$ chimaeras (Fig. 2i). Moreover, when SatM were co-cultured with lung fibroblasts, these fibroblasts significantly upregulated *Spp1* mRNA (Fig. 2j). To elucidate the mechanism of *Spp1* induction in activated fibroblasts and SatM, we measured several cytokines produced by SatM. We noted that SatM produced large amounts of TNF-α (Extended Data Fig. 7a). In addition, as *Spp1* mRNA expression was partially upregulated in fibroblasts stimulated with TNF-α (Extended Data Fig. 7b), it can be hypothesized that SatM are crucial for the induction of activated fibroblasts followed by the beginning of fibrosis, at least in part, through production of TNF-α by SatM. However, the production of additional factors by SatM may also be important for fibrosis development. Finally, we confirmed that *Spp1* and *Tnf* (also known as *Tnfa*) mRNA induction (Fig. 2k, l) and TGF-β production (Fig. 2m) were restored in bleomycin-treated *Cebpb*$^{-/-}$ chimaeras transplanted with SatM. Collectively, these findings demonstrate that the resistance to fibrosis observed in *Cebpb*$^{-/-}$ chimaeras is intrinsic to haematopoietic cells, and that C/EBPβ plays a crucial role in regulating the differentiation of SatM. Furthermore, these cells activate fibroblasts to initiate fibrosis.

[1]Laboratory of Host Defense, World Premier Institute Immunology Frontier Research Center, Osaka University, Osaka, 565-0871, Japan. [2]Department of Host Defense, Research Institute for Microbial Diseases (RIMD), Osaka University, Osaka, 565-0871, Japan. [3]Laboratory of Biofunctional Imaging, World Premier Institute Immunology Frontier Research Center, Osaka University, Osaka, 565-0871, Japan. [4]Research Center for Ultra-high Voltage Electron Microscopy, Osaka University, Osaka, 567-0047, Japan. [5]Discovery Research Department, Research Division, Chugai Pharmaceutical Co., Ltd., Kanagawa, 247-8530, Japan. [6]Core Research for Evolutional Science and Technology, Japan Agency for Medical Research and Development, Tokyo, 100-0004, Japan. [7]Department of Respiratory Medicine, Allergy and Rheumatic Diseases, Graduate School of Medicine, Osaka University, Osaka, 565-0871, Japan.
*These authors contributed equally to this work.

© 2016 Macmillan Publishers Limited, part of Springer Nature. All rights reserved.

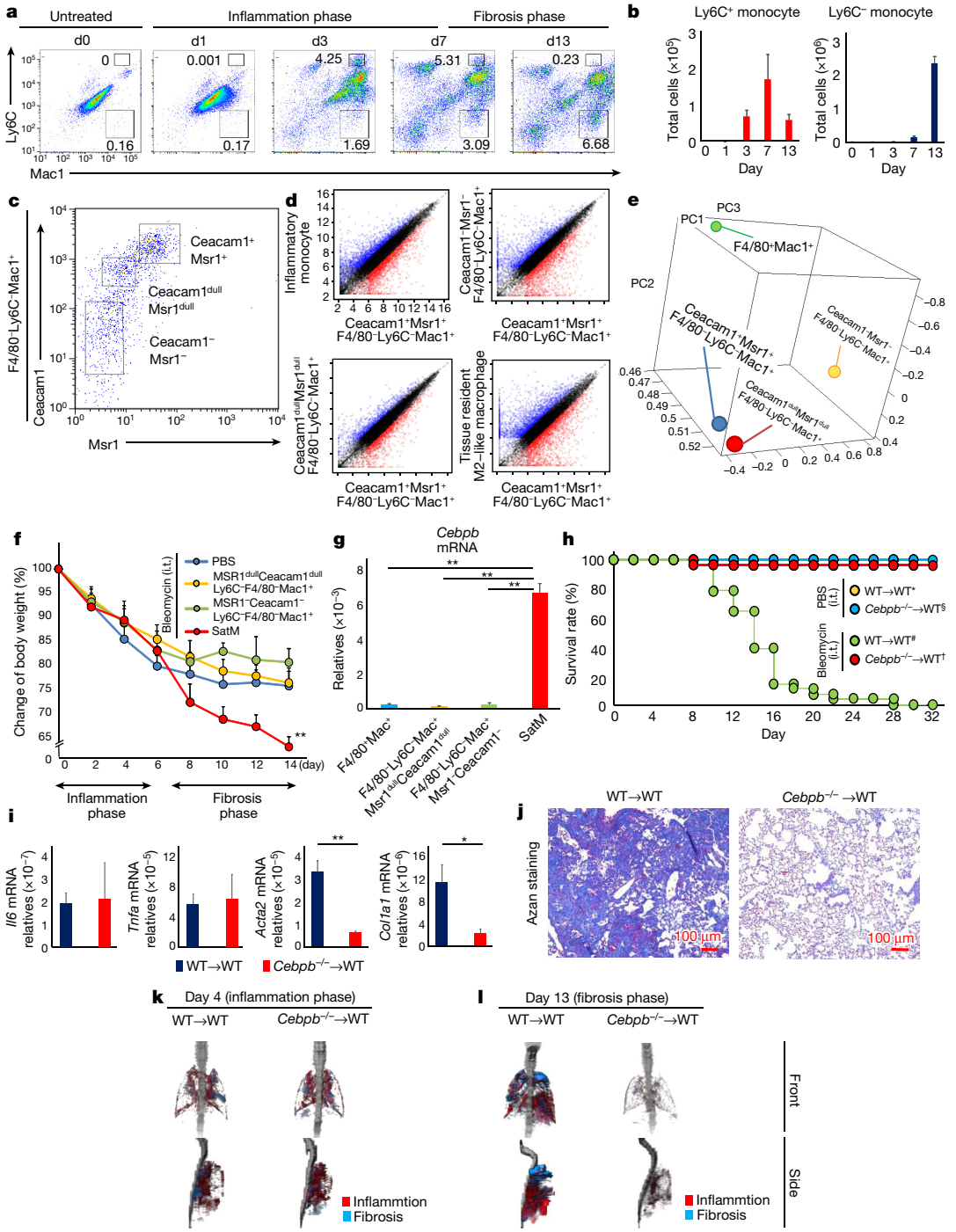

Figure 1 | *Cebpb*$^{-/-}$ chimaeric mice are resistant to fibrosis. a, FACS analysis of bronchial-alveolar lavage (BAL) from bleomycin-treated wild-type mice. **b**, Total numbers of each cell subset from **a**. **c**, The three groups are present in the Ly6C^{-} population. Similar results were obtained in five independent experiments (**a**–**c**). **d**, **e**, Scatter plot analysis (**d**) and principal component analysis (PCA) (**e**). **f**, Body weight changes. **g**, *Cebpb* expression of indicated subsets. Error bars indicate the s.d. in duplicate. **h**, The survival rate of bleomycin-inoculated indicated chimaeras ($n = 28$); log-rank test, *, § and † $P < 0.01$ versus #. **i**, Indicated mRNA levels in BAL by qPCR. Error bars indicate the s.d. in duplicate. Similar results were obtained in three independent experiments (**f**–**i**). **j**, Azan and haematoxylin and eosin (H&E) staining images. **k**, **l**, Spatio-temporal 3D analysis at day 4 (**k**) and day 13 (**l**). Similar results were obtained in five independent experiments (**j**–**l**). Statistical significance was determined using Student's *t*-test (**f**, **g**, **i**), $*P < 0.05$, $**P < 0.01$.

FACS analysis of SatM in the bone marrow clearly showed monocyte characteristics (Extended Data Fig. 8a, b). Interestingly, in addition to M-CSFR (macrophage colony-stimulating factor receptor), characteristic granulocyte markers were also expressed on SatM (Fig. 3a, Extended Data Fig. 8a–d). Consistent with these results, SatM expressed granulocyte-related genes as well as monocyte-related genes, but inflammatory monocytes did not (Fig. 3b). Moreover, whole-cell proteomics analysis and immunostaining of SatM clearly showed that various granule proteins were present (Fig. 3c, Extended Data Fig. 8e). However, although SatM clearly demonstrated common characteristics between monocytes and granulocytes, principal component analysis and morphological data demonstrated that these cell types were completely different from typical granulocytes (Fig. 3d, Extended Data Fig. 8f–h).

© 2016 Macmillan Publishers Limited, part of Springer Nature. All rights reserved.

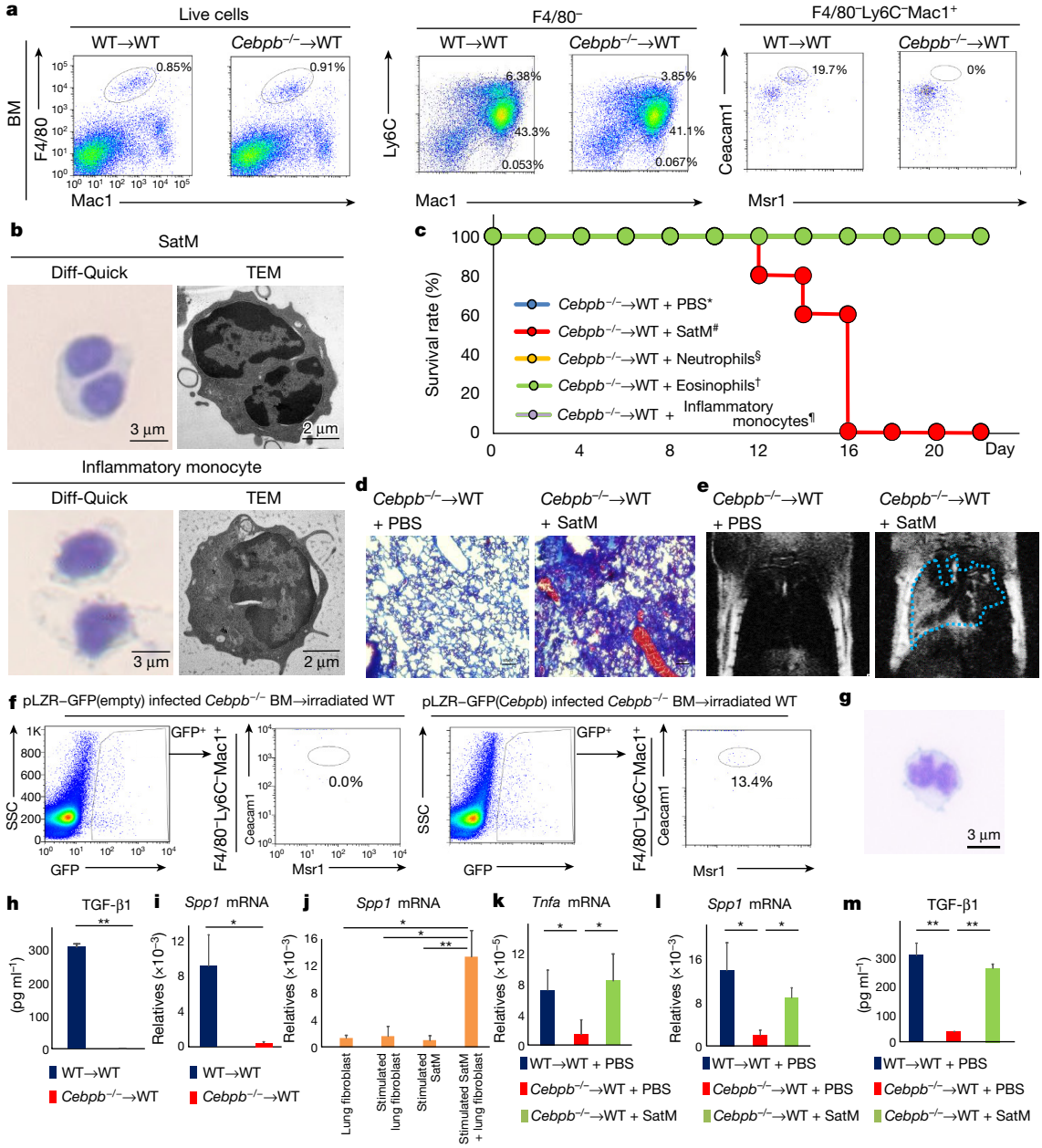

Figure 2 | Critical role of C/EBPβ in the differentiation of SatM. **a**, FACS of bone marrow (BM) from indicated mice. **b**, Images of Diff-Quick staining and transmission electron microscopy (TEM) of SatM and inflammatory monocyte. **c**, Survival rate; log-rank test, *, §, † and ¶ $P < 0.01$ versus #. **d**, **e**, Images of Azan staining (**d**) and MRI analysis (**e**) of lung. **f**, **g**, FACS analysis of *Cebpb*$^{-/-}$ chimeric mice reconstituted with indicated vectors. **g**, Restored SatM in **f** are stained with Diff-Quick. **h**, TGF-β1 level in BAL in the fibrotic phase. **i**, *Spp1* mRNA levels of lungs in early fibrotic phase were determined by qPCR in triplicate. **j**, *Spp1* mRNA was determined by qPCR in triplicate. **k**, **l**, Levels of *Tnfa* mRNA in BAL (**k**) and *Spp1* mRNA in lungs (**l**) in early fibrotic phase by qPCR in duplicate. **m**, TGF-β1 in BAL in the fibrotic phase. Results are representative of three (**a**, **b**, **h**–**m**) or at least two (**c**–**g**) independent experiments. Statistical significance was determined using the Student *t*-test, * $P < 0.05$, ** $P < 0.01$. Error bars indicate the s.d. (**h**–**m**).

As SatM were absent in the bone marrow of *Cebpb*$^{-/-}$ chimaeric mice, these data prompted us to investigate the point of action of C/EBPβ in differentiation of SatM by examining progenitors of SatM. First, adoptive transfer of granulocyte/macrophage progenitors (GMPs) showed differentiated SatM, inflammatory monocytes and neutrophils (Fig. 3e). In contrast, adoptive transfer of macrophage/dendritic-cell progenitors (MDPs) did not result in the differentiation of SatM. Notably, the proportions of GMPs and MDPs were comparable between wild-type mice and *Cebpb*$^{-/-}$ chimaeras (Extended Data Fig. 9a), suggesting that C/EBPβ regulates SatM differentiation downstream of GMPs, but not of MDPs/cMoPs (common monocyte progenitors). As GMPs can be divided into Ly6C^{+} and Ly6C^{-} subpopulations[11], each GMP subtype was adoptively transferred into mice and SatM was differentiated from Ly6C^{-} GMPs (Fig. 3f), suggesting that SatM are derived from Ly6C^{-} GMPs, but not MDPs or Ly6C^{+} GMPs.

Given that Ly6C^{-} GMPs are also a heterogenic population, we further divided these cells. To classify Ly6C^{-} GMPs, cell surface markers of SatM in bone marrow were used. Thus, GMPs were divided into three populations using the selected granulocyte marker FcεRI (Fig. 3g). We found that Ly6C^{-}FcεRI^{-} GMPs gave rise to Ly6C^{+}FcεRI^{-} GMPs *in vitro*. By contrast, the Ly6C expression did not change in Ly6C^{-}FcεRI^{+} GMP (Fig. 3h). Although adoptive transfer of Ly6C^{-}FcεRI^{+} GMPs showed differentiation of SatM *in vivo*, transfer of *Cebpb*$^{-/-}$ Ly6C^{-}FcεRI^{+}

© 2016 Macmillan Publishers Limited, part of Springer Nature. All rights reserved.

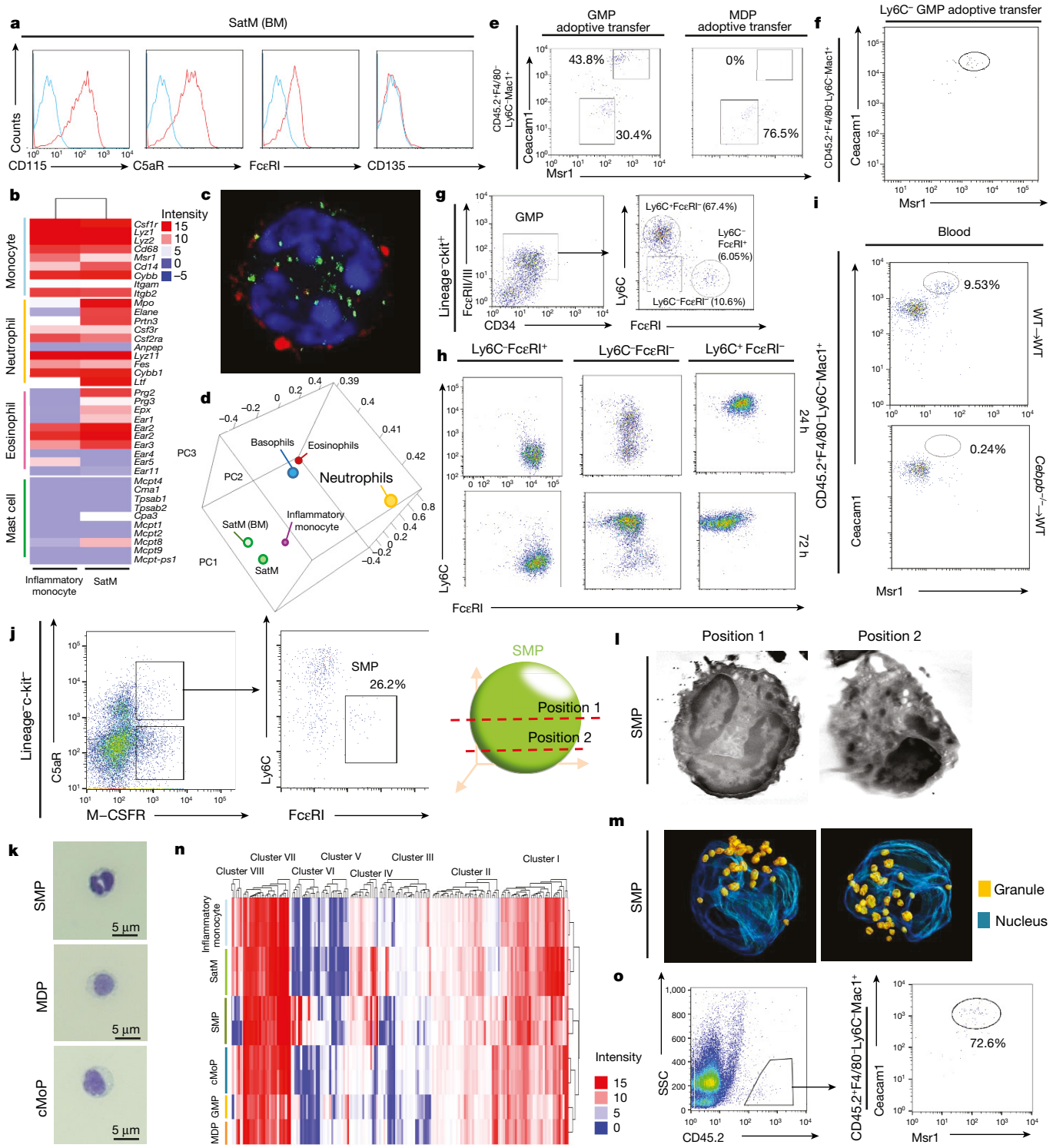

Figure 3 | Identification of SatM progenitor cells. a, Surface receptor expression of SatM in the bone marrow. Similar results were obtained in three independent experiments. **b**, Microarray analysis of indicated cell markers. **c**, SatM were stained for neutrophil elastase (green), lactotransferrin (red) and with DAPI (blue). **d**, PCA of indicated cell types. **e**, **f**, FACS analysis of GMPs (**e**, left), MDPs (**e**, right) and Ly6C$^-$ GMPs (**f**) adoptive transfer. **g**, Ly6C and FcεRI expression in GMPs. **h**, Development of indicated cells from corresponding progenitors. **i**, Development of SatM from wild-type and *Cebpb*$^{-/-}$ Ly6C$^-$FcεRI$^+$ GMPs *in vivo*. **j**, FACS analysis of SMPs. **k**, Indicated progenitors stained with Diff-Quick. **l**, **m**, SMPs were imaged by scanning TEM (**l**) and 3D reconstruction (**m**). **n**, Heatmap of the transcription factor. **o**, FACS analysis of SMP adoptive transfers. Similar results were obtained in three independent experiments (**c**–**o**).

GMPs did not (Fig. 3i). Furthermore, May–Giemsa staining clearly showed that cells, in a similar manner to SatMs in bone marrow, were contained within this Ly6C$^-$FcεRI$^+$ GMP subset (Extended Data Fig. 9b). We next classified the SatM progenitor downstream of Ly6C$^-$FcεRI$^+$ GMPs. We identified a novel myeloid cell progenitor fraction, which was characterized as lineage-negative (Lin$^-$), CD117 (c-kit)$^-$, C5aR$^+$, M-CSFR$^+$, FcεRI$^+$ and Ly6C$^-$ (Fig. 3j). May–Giemsa staining and 3D tomographic imaging clearly showed that these progenitors were morphologically analogous to SatM (Figs 3k–m; Supplementary Videos S6, S7). Moreover, hierarchical

© 2016 Macmillan Publishers Limited, part of Springer Nature. All rights reserved.

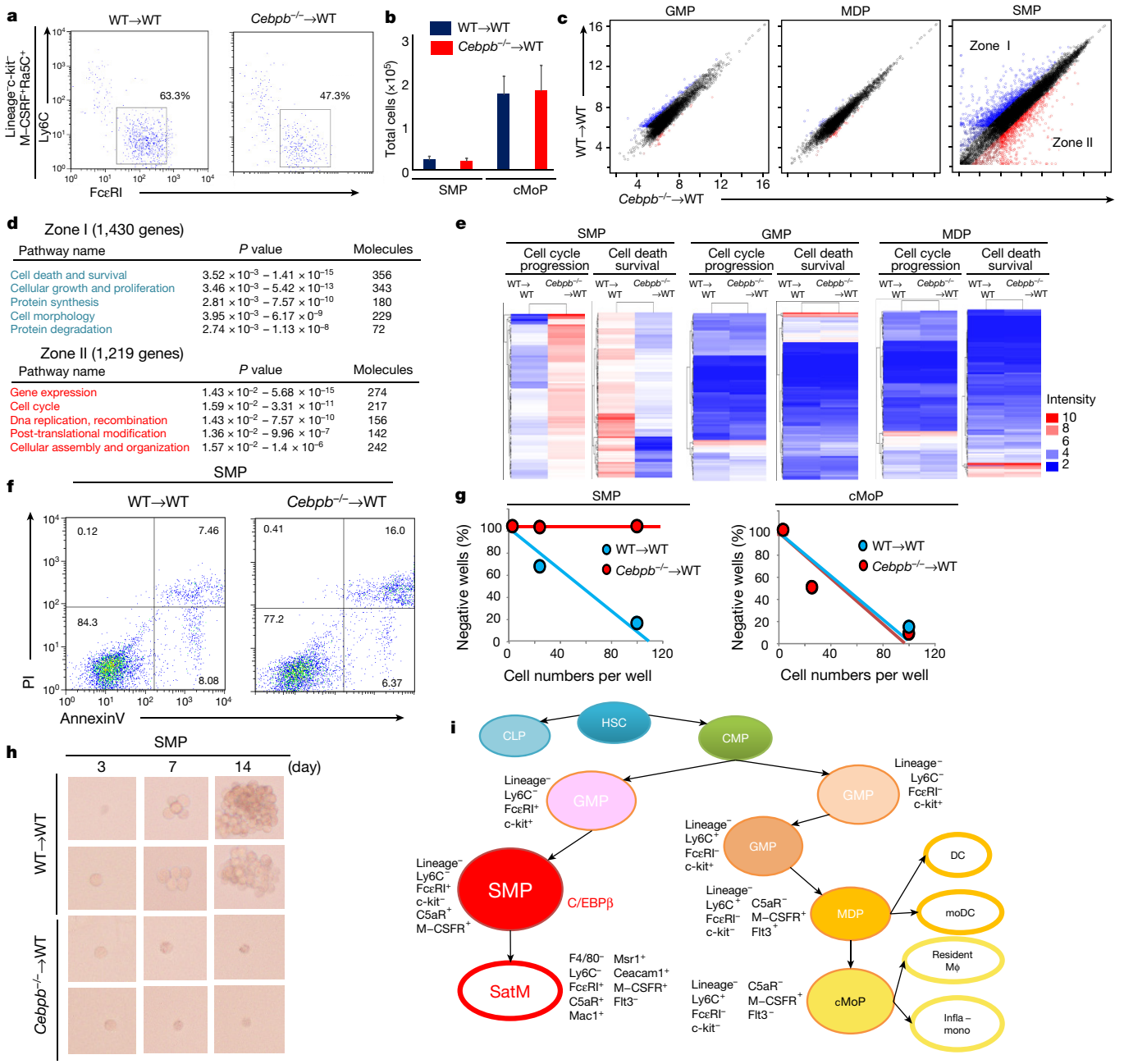

Figure 4 | C/EBPβ licenses SatM differentiation from committed progenitor cells. a, FACS analysis of SMPs. **b**, The total numbers of SMPs and cMoPs. Similar results were obtained in three independent experiments. **c**, Scatter plot analysis of the indicated cell type. **d**, **e**, Microarray data were used for pathway analysis (**d**) and a heatmap of indicated cell subsets (**e**). **f**, FACS analysis of dead cells in wild-type and *Cebpb*$^{-/-}$ SMP cultures. **g**, **h**, Colony-forming assays of indicated progenitor cells, the number of colonies counted (**g**), and images of the proliferated colonies captured (**h**). Similar results were obtained in three independent experiments (**f**–**h**). **i**, Schematic diagram of SatM differentiation.

clustering analysis demonstrated that the SatM progenitors expressed several genes involved in monocyte/macrophage development, including *Klf4*, *Sfpi1* and *Cebpb*[9]. Interestingly, the progenitors also highly expressed *Gata1* and *Gata2*, which are critical for granulocyte differentiation[12–14]. The expression of *Irf8*, which is important in the differentiation balance of granulocytes and macrophages[11,15], was suppressed in SatM progenitors (Fig. 3n, Extended Data Fig. 9c, d). Finally, adoptive transfer of SatM progenitor cells led to the appearance of SatM cells (Fig. 3o, Extended Data Fig. 9e). All findings indicated that the progenitor cell, which is distinct to cMoPs and MDPs, gives rise to SatM and we termed this novel population SatM progenitors (SMPs).

To investigate whether C/EBPβ acts on SMPs, we compared each progenitor in wild-type and *Cebpb*$^{-/-}$ chimaeras. The total cell number and ratio of SMPs, GMPs and MDPs were comparable between wild-type and *Cebpb*$^{-/-}$ chimaeras (Fig. 4a, b, Extended Data Fig. 9a). Interestingly, the gene expression pattern in *Cebpb*$^{-/-}$ SMPs, but not GMPs and MDPs, was very different from wild type (Fig. 4c). Among these genes, bioinformatic functional analysis using Ingenuity Pathway Analysis (IPA) showed that a cluster of cell death pathways was significantly affected by *Cebpb* deficiency (Fig. 4d, e). Consistent with this result, *Cebpb*-deficient SMP cultures contained significantly more dead cells (Fig. 4f). Whereas cMoPs developed normally, *Cebpb*$^{-/-}$ SMP colonies did not completely proliferate (Fig. 4g, h). Collectively, these findings indicated that C/EBPβ controls SatM differentiation at the SMP stage, downstream of Ly6C^{-}FcεRI^{+} GMPs (Fig. 4i).

It is recognized that Ly6C^{-} populations are converted from differentiated Ly6C^{+} populations in the periphery[16–18]. Indeed, Ly6C^{+} monocytes/macrophages give rise to Ly6C^{-} cells through the

© 2016 Macmillan Publishers Limited, part of Springer Nature. All rights reserved.

GMP–MDP–cMoP axis[19,20]. However, our research showed that the Ly6C expression remains low even in SMPs, as well as Ly6C$^-$FcεRI$^+$ GMPs and SatM. Therefore, despite some Ly6C$^-$ monocyte/macrophage subsets being differentiated from Ly6C$^+$ monocytes, Ly6C$^-$ SatM are differentiated through a Ly6C$^-$FcεRI$^+$ GMP–SMP axis without conversion of Ly6C expression.

We previously reported two disorder-related macrophage subtypes regulated by Trib1 and Jmjd3 respectively[21,22]. We found that *Trib1*$^{-/-}$ and *Jmjd3*$^{-/-}$ chimaeras did not show any defects in SatM and fibrosis development (Extended Data Fig. 10a–c). Similarly, *Cebpb*$^{-/-}$ chimaeras showed eosinophil recruitment by corresponding macrophages to allergic stimuli and did not show any development of lipodystrophy. Thus, monocytes and macrophages can be categorized into several distinct phenotypes and their respective differentiation mechanisms are known[1–4,21–23]. However, in previous studies, the terminology of M1 and M2 macrophages is still widely and ambiguously used. This is based on the idea that macrophages are a single entity and display a high plasticity of the phenotype in various local environments. However, such simple classification should be questioned. Accumulating evidence from recent studies suggests that monocytes and macrophages are composed of multiple subsets with functional diversity, indicating that macrophage subtypes should be redefined depending on their characteristics and corresponding disorders. Given that 'disorder-specific monocyte/macrophage subtypes' corresponding to certain diseases have been identified, investigated and regulated, it may also now be possible to develop novel, more specific therapeutic targets with fewer side effects.

Online Content Methods, along with any additional Extended Data display items and Source Data, are available in the online version of the paper; references unique to these sections appear only in the online paper.

Received 23 February; accepted 7 November 2016.
Published online 21 December 2016.

1. Asano, K. *et al.* CD169-positive macrophages dominate antitumor immunity by crosspresenting dead cell-associated antigens. *Immunity* **34,** 85–95 (2011).
2. Auffray, C. *et al.* Monitoring of blood vessels and tissues by a population of monocytes with patrolling behavior. *Science* **317,** 666–670 (2007).
3. Kohyama, M. *et al.* Role for Spi-C in the development of red pulp macrophages and splenic iron homeostasis. *Nature* **457,** 318–321 (2009).
4. Okabe, Y. & Medzhitov, R. Tissue-specific signals control reversible program of localization and functional polarization of macrophages. *Cell* **157,** 832–844 (2014).
5. Swirski, F. K. *et al.* Identification of splenic reservoir monocytes and their deployment to inflammatory sites. *Science* **325,** 612–616 (2009).
6. Duffield, J. S., Lupher, M., Thannickal, V. J. & Wynn, T. A. Host responses in tissue repair and fibrosis. *Annu. Rev. Pathol.* **8,** 241–276 (2013).
7. Sica, A., Invernizzi, P. & Mantovani, A. Macrophage plasticity and polarization in liver homeostasis and pathology. *Hepatology* **59,** 2034–2042 (2014).
8. Wynn, T. A., Chawla, A. & Pollard, J. W. Macrophage biology in development, homeostasis and disease. *Nature* **496,** 445–455 (2013).
9. Sheel, M. & Engwerda, C. R. The diverse roles of monocytes in inflammation caused by protozoan parasitic diseases. *Trends Parasitol.* **28,** 408–416 (2012).
10. Tsukui, T. *et al.* Qualitative rather than quantitative changes are hallmarks of fibroblasts in bleomycin-induced pulmonary fibrosis. *Am. J. Pathol.* **183,** 758–773 (2013).
11. Yáñez, A., Ng, M. Y., Hassanzadeh-Kiabi, N. & Goodridge, H. S. IRF8 acts in lineage-committed rather than oligopotent progenitors to control neutrophil vs monocyte production. *Blood* **125,** 1452–1459 (2015).
12. Arinobu, Y., Iwasaki, H. & Akashi, K. Origin of basophils and mast cells. *Allergol. Int.* **58,** 21–28 (2009).
13. Li, Y., Qi, X., Liu, B. & Huang, H. The STAT5–GATA2 pathway is critical in basophil and mast cell differentiation and maintenance. *J. Immunol.* **194,** 4328–4338 (2015).
14. Nei, Y. *et al.* GATA-1 regulates the generation and function of basophils. *Proc. Natl Acad. Sci. USA* **110,** 18620–18625 (2013).
15. Scheller, M. *et al.* Altered development and cytokine responses of myeloid progenitors in the absence of transcription factor, interferon consensus sequence binding protein. *Blood* **94,** 3764–3771 (1999).
16. Gutknecht, M. F. & Bouton, A. H. Functional significance of mononuclear phagocyte populations generated through adult hematopoiesis. *J. Leukoc. Biol.* **96,** 969–980 (2014).
17. Terry, R. L. & Miller, S. D. Molecular control of monocyte development. *Cell. Immunol.* **291,** 16–21 (2014).
18. Yona, S. *et al.* Fate mapping reveals origins and dynamics of monocytes and tissue macrophages under homeostasis. *Immunity* **38,** 79–91 (2013).
19. Auffray, C. *et al.* CX3CR1$^+$CD115$^+$CD135$^+$ common macrophage/DC precursors and the role of CX3CR1 in their response to inflammation. *J. Exp. Med.* **206,** 595–606 (2009).
20. Hettinger, J. *et al.* Origin of monocytes and macrophages in a committed progenitor. *Nat. Immunol.* **14,** 821–830 (2013).
21. Satoh, T. *et al.* Critical role of Trib1 in differentiation of tissue-resident M2-like macrophages. *Nature* **495,** 524–528 (2013).
22. Satoh, T. *et al.* The Jmjd3-*Irf4* axis regulates M2 macrophage polarization and host responses against helminth infection. *Nat. Immunol.* **11,** 936–944 (2010).
23. Hanna, R. N. *et al.* The transcription factor NR4A1 (Nur77) controls bone marrow differentiation and the survival of Ly6C$^-$ monocytes. *Nat. Immunol.* **12,** 778–785 (2011).

Supplementary Information is available in the online version of the paper.

Acknowledgements We thank S. Saeki, S. Watanabe, R. Takenaka and M. Miyamoto for assistance with experiments, and T. Matsuki, T. Kawasaki, H. Kanemaru, H. Tanaka and K. Kuniyoshi for helpful discussions. We thank T. Kitamura for providing PlatE cells. We also thank E. Kamada for secretarial assistance, and C. Funamoto, N. Kitagaki, A. Wataki, K. Yokoyama and R. Kawaguchi for technical assistance. This work was supported by the Government of Japan and the Japan Society for the Promotion of Science (JSPS) through the funding program for World-Leading Innovative R&D on Science and Technology (FIRST Program), by Japan Science and Technology Agency (JST) thorough funding for a Grant-in-Aid for Young Scientists (A) (16H06234), Specially Promoted Research (15H05704) and the US National Institutes of Health (P01-AI070167) and 'Visionary Research Fund' from Takeda Science Foundation. A part of this work was supported by the Nanotechnology Platform (project number 12024046) of the Ministry of Education, Culture, Sports, Science and Technology (MEXT), Japan.

Author Contributions T.S. designed and performed the experiments and wrote the manuscript. K.F., I.E., F.Y. and A.K. helped with experiments. K.N. performed the experiments. M.A. and Y.M. performed bioinformatics analysis. F.S. and Y.Y. performed the MRI analysis. R.K. performed the electron microscopy analysis. S.A. wrote the manuscript and supervised the project.

Author Information Reprints and permissions information is available at www.nature.com/reprints. The authors declare competing financial interests: details are available in the online version of the paper. Readers are welcome to comment on the online version of the paper. Correspondence and requests for materials should be addressed to S.A. (sakira@biken.osaka-u.ac.jp).

Reviewer Information *Nature* thanks I. Amit, D. Brenner, F. Geissmann and the other anonymous reviewer(s) for their contribution to the peer review of this work.

© 2016 Macmillan Publishers Limited, part of Springer Nature. All rights reserved.

METHODS

Animal husbandry and ethics. Mice were housed in individually ventilated cages in a temperature and light regulated room in a SPF facility and received food and water *ad libitum*. All studies received local ethics review board approval and were performed in accordance with the guidelines of the animal care and use committee of the Research Institute for Microbial Diseases at Osaka University. The experiments were not randomized and the investigators were not blinded to allocation during experiments and outcome assessment.

Mice. *Cebpb*$^{-/-}$ mice were prepared as described previously[24]. Fetal liver cells were prepared from CD45.2^{+} wild-type and *Cebpb*$^{-/-}$ embryos (E15.5). The cell suspensions were intravenously injected into lethally irradiated CD45.1^{+} C57BL/6 male mice. The chimaeric mice were given neomycin and ampicillin in their drinking water for 4 weeks. The mice were analysed at least 8 weeks after reconstitution. More than 90% of splenocytes from chimaeric mice were CD45.2 positive. *Cebpd*$^{-/-}$ mice were prepared as described previously[25]. *Jmjd3*$^{-/-}$ mice and *Trib1*$^{-/-}$ mice were prepared as described previously[22,23]. Eosinophil-deficient ΔdblGATA mice were purchased from Jackson Laboratory (Bar Harbour, Maine, USA).

Immunoblot analysis. SatM were cultured for 4 h in medium without M-CSF (PeproTech), then collected and replated. SatM were stimulated with M-CSF for the indicated time and lysed with lysis buffer (20 mM Tris-HCl (pH 7.5), 150 mM NaCl, 1 mM EDTA and 1% (vol/vol) Nonidet P-40) containing complete mini protease inhibitor cocktail (Roche). Cell lysates were separated by SDS–PAGE and analysed by immunoblot. Antibodies to the following proteins were used: phosphorylated Erk (9101; Cell Signaling Technology), phosphorylated Akt (9271; Cell Signaling Technology), Akt (9272; Cell Signaling Technology), Erk (K-23; Santa Cruz Biotechnology) and β-actin (C-11; Santa Cruz).

Quantitative PCR analysis. Total RNA was isolated using a RNA purification kit (Roche) and reverse transcription was performed with ReverTraAce (Toyobo) according to the manufacturer's instructions. For quantitative PCR, cDNA fragments were amplified with real-time PCR Master mix (Toyobo), and fluorescence from the TaqMan probe for each cytokine detected with a 7500 real-time PCR system (Applied Biosystems). To determine the relative induction of cytokine mRNA in response to various stimuli, the mRNA expression level of each gene was normalized to the expression level of 18S RNA. The accession number of TaqMan probes were below; *Acta2*: Mm00725412_s1, *Col1a1*: Mm00801666_g1, *Spp1*: Mm00436767_m1, *Cebpb*: Mm00843434_s1, *il6*: Mm00446190_m1, *Tnfa*: Mm00443258_m1, *Tgfb1*: Mm01178820_m1.

Flow cytometry and cell sorting. Antibodies for flow cytometry were purchased from commercial sources as follows: anti-F4/80 (BM8; BioLegend); anti-Mac1 (M1/70; BioLegend); anti-Ly6C (AL-21; BioLegend); anti-Siglec-F (E50-2446; BD Biosciences); anti-CCR3 (83103; BD Biosciences); anti-CD206 (MR5D3; BioLegend); anti-CD11c (N418; BioLegend); anti-CD117 (c-kit) (ACK2; BioLegend); anti-Ly-6A/E (Sca-1) (D7; BioLegend); anti-FcεRI (MAR-1; BioLegend); anti-CD88 (C5aR) (20/70; BioLegend); anti-CD66a (Ceacam1) (Mab-CC1; BioLegend); anti-CD115 (M-CSFR) (AFS98; BioLegend); anti-CD135 (A2F10; BioLegend); and anti-Msr1 (LS-c43466; LSBio). Cell suspensions were prepared by sieving and gentle pipetting. Cells were washed in ice-cold FACS buffer (2% FCS, 2 mM EDTA in PBS), then incubated with each antibody for 15 min and washed twice with FACS buffer. Data were acquired on a FACS Canto II flow cytometer and Aria III (BD), and analysed using FlowJo (Tree Star Inc.). For FACS analysis and sorting of progenitor cells, before application, bone-marrow cells were purified by lineage cell depletion kit (130-090-858; Miltenyi Biotec).

Construction of *Cebpb* expression plasmids. *Cebpb* cDNA was obtained by PCR from a mouse cDNA library. The full *Cebpb* cDNAs were cloned into the pLZR-ires-GFP vector for retrovirus production.

Retroviral transduction. Fetal liver cells were collected from *Cebpb*$^{-/-}$ mice. Cells were cultured in stem-cell media (RPMI supplemented with 15% FCS, 10 mM sodium pyruvate, 2 μM L-glutamine, 50 μM β-mercaptoethanol, 100 U ml^{-1} penicillin, 100 μg ml^{-1} streptomycin, 100 ng ml^{-1} SCF, 10 ng ml^{-1} IL-6 and 10 ng ml^{-1} IL-3). Then, 48 h later, these cells were transduced with retroviral supernatant (supplemented with SCF, IL-6, IL-3 and RetroNectin) on two successive days. Virus was produced using PlatE packaging cells transfected with various plasmids. After the second transduction, cells were washed and resuspended in macrophage growth media (RPMI 1640 medium supplemented with 10% FCS, 50 μM β-mercaptoethanol, 100 U ml^{-1} penicillin and 100 μg ml^{-1} streptomycin). After infection, cells were washed three times and intravenously injected into lethally irradiated CD45.1^{+} C57BL/6 mice. The chimaeric mice were given neomycin and ampicillin in their drinking water for 2 weeks. The mice were analysed at least 4 weeks after reconstitution.

Examination of fibrosis development after bleomycin administration and SatM adoptive transplantation. Mice were anaesthetized with 1.0–1.5% sevoflurane during the bleomycin administration. Bleomycin (3 μg per g body weight) was administrated to the mice intratracheally.

For SatM adoptive transplantation, bone-marrow cells were collected from wild-type mice. After MACS purification, SatM, neutrophils, eosinophils and inflammatory monocytes were sorted by Aria III. These cell types (2×10^6 cells per mouse) were administered twice to the mice intravenously (on days 0 and 7).

SatM and lung fibroblast co-culture assay. Lung fibroblasts (1×10^5 cells per well) were seeded into 24-well plates and cultured with or without zymosan (10 μg ml^{-1}) stimulated SatM (1×10^5 cells per well). After 72 h culture, RNA was purified from these cells and qPCR analysis performed.

***In vitro* GMP sub-population differentiation assay.** Isolated progenitors (2×10^5 cells per well) were seeded in 24-well plates with RPMI medium with IL-3 (10 ng ml^{-1}) and IL-6 (20 ng ml^{-1}) (R&D Systems). Cells were collected and analysed by flow cytometry at the indicated time point.

***In vitro* SMP differentiation assay.** Bone-marrow cells (2×10^3) were seeded into 96-well plates and cultured for 14 days with SCF, IL-6 and IL-3 containing Methocult (3534; Stem Cell Technologies) in the presence of 20 ng ml^{-1} M-CSF. The numbers of wells containing proliferated colonies were counted for colony-forming assays.

***In vivo* progenitor differentiation.** Progenitors were collected by cell sorting (FACSAria III, Becton Dickinson). Before cell sorting, bone-marrow cells were subjected to MACS to enrich for lineage negative cells (lineage markers: CD3, CD19, B220, Ter119, DX5, Mac1, F4/80 and CD11c). Progenitors (2×10^5 cells in 100 μl PBS per mouse) obtained from CD45.2^{+} mice were injected into CD45.1^{+} recipient mice. Mice were killed after 4 days and the collected tissues were analysed by FACS before flow cytometric analysis to enrich CD45.2^{+} cells.

Transmission electron microscopy. Transmission electron microscope observations were carried out as described previously with some modifications[26]. The cells were fixed with 2.5% glutaraldehyde, 2% paraformaldehyde and 0.1 M phosphate buffer. After fixation with 1% osmium tetroxide for 1 h, the cells were dehydrated through a graded series of ethanol (30–100%) and propylene oxide. Finally, the cells were embedded in epoxy resin. Sections were cut on an ultramicrotome (EM UC7, Leica) and stained with uranyl acetate and lead citrate. The sections were observed by transmission electron microscope (H-7500; Hitachi High-Technologies).

Scanning transmission electron microscope tomography. Scanning TEM tomography observation was carried out as described previously with some modifications[27]. Sections (1 μm thick) were cut and observed by 200 kV scanning transmission electron microscope (Tecnai G2; FEI). The images were collected covering an angular range from −70° to +70° with a nonlinear Saxton tilt scheme using the Xplore 3D software package (FEI). 3D reconstructions were calculated using the IMOD software package[28].

Microarray analysis. Total RNA was isolated from each myeloid cell sample using a RNA isolation kit (Roche) and further purified using a RNeasy kit (Qiagen). Biotinylated cDNA was synthesized from 50 ng total RNA using Ovation biotin RNA amplification and labelling systems (NuGEN Technologies Inc.) according to the manufacturer's protocol. The product was purified using a DyeEx2.0 spin kit (Qiagen), fragmented, and hybridized on mouse expression microarray chips (Mouse Genome A430 2.0; Affymetrix), after which the microarray chips were stained, washed, and scanned according to the manufacturer's instructions. Background-adjusted robust multichip average expression values were calculated using the 'gcrma' package in R. After $\log_2$ transformation of the data, differentially expressed genes between the two samples were selected on the basis of the fold change (1 or −1 at $\log_2$ level) and the detection limit (set at 6 at a $\log_2$ level). Genes were assigned the values of their corresponding probe, and where a gene was associated with multiple probes the maximum value was taken. The probes that had expression values over the detection limit in at least one sample were used for further analyses, such as scatterplot analysis, principal component analysis, pathway analysis, and heatmap analysis. For the heatmap analysis on progenitor and/or peripheral myeloid cells, granulopoietin genes and transcription factor genes were listed manually from various references and the Transcription Factor Encyclopaedia (http://www.cisreg.ca/tfe), respectively, and then transformed into probes using an annotation file provided by Affymetrix on NetAffy (http://www.affymetrix.com). Selected probes were depicted without or with *k*-mean clustering by the 'ComplexHeatmap' package in R. The pathway analysis on wild-type and *Cebpb*$^{-/-}$ samples (Core Analysis in Ingenuity Pathway Analysis; Qiagen) extracted pathways in which differentially expressed genes were significantly concentrated. Probes based on selected genes from the pathways were depicted in a heatmap analysis.

Whole-cell proteomics of SatM. SatM from bone marrow were lysed in a buffer containing 1% NP-40, 150 mM NaCl, 50 mM Tris-Cl (pH 7.5) and a protease inhibitor cocktail (Roche Diagnostics). Proteins were precipitated from the cell lysate with methanol and chloroform and then suspended in a buffer containing

© 2016 Macmillan Publishers Limited, part of Springer Nature. All rights reserved.

8 M urea and 400 mM NH_4HCO_3. Protein samples were then reduced, alkylated, and digested with trypsin (Promega). Tryptic digests were then desalted and concentrated using a Monospin C18 (GL Science) and the samples were subjected to LC-MS/MS (liquid chromatography–tandem mass spectrometry) analysis comprises Q-Exactive (Thermo Scientific) and the nano-LC system, Ultimate 3000 (Thermo Scientific). Protein identification and quantification were carried out by MaxQuant software.

Magnetic resonance imaging. An AvanceIII BioSpec 117/11 system (Bruker) equipped with ^{1}H QD coil was used for MRI imaging. Mice were anaesthetized with sevoflurane during the imaging process and body temperature maintained with a warm water circulating tube. Fast spin echo protocol (RARE) was used for T1 weight, T2 weight and water suppression (WS) imaging. Acquired images were converted to DICOM format and processed by ImageJ (NIH, Bethesda) for 3D reconstruction. Final images were processed by Imaris software (Bitplane AG), with inflammation and fibrosis coloured as red and blue, respectively. The MRI parameters were as follows: time 1 (T1) weight, time 2 (T2) weight, TR/TE (time of repetition/time of echo) = 3,500 per 36 ms, 12 times average; and WS, TR/TE = 800 per 12 ms, 10 times average. The image matrix was 256 × 128 and field of view 4 cm × 3 cm; 16 slices were acquired with slice thickness 1.2 mm. Fat suppression was applied for all images. The suppression pulse used for WS image was gauss shape with width 1 kHz, offset at −300 Hz from water peak. More details are described in Extended Data Fig. 2.

Cutaneous wound healing model. Mice were anaesthetized with isoflurane, their backs were shaved and any remaining hair removed with depilatory cream (Epilat, Kracie Holdings). Two full-thickness excisional skin wounds were made on either side of the dorsal midline using a disposable sterile 6-mm biopsy punch (Kai Industries). Each wound was digitally photographed at the indicated time intervals, and the respective wound area (mm^2) was calculated with ImageJ software (version 1.48j, NIH) using a constant reference.

Statistical analysis. The statistical significance of differences between groups was calculated using the two-tailed Student's *t*-test, and survival curves were analysed by the log-rank test. *P* values of $*P < 0.05$, $**P < 0.01$ were considered to indicate statistical significance. No statistical methods were used to predetermine sample size. No animal or sample was excluded from the analysis.

Data availability. The data sets generated during and analysed during the current study are available from the corresponding author on reasonable request.

24. Tanaka, T. *et al.* Targeted disruption of the NF-IL6 gene discloses its essential role in bacteria killing and tumor cytotoxicity by macrophages. *Cell* **80,** 353–361 (1995).
25. Tanaka, T., Yoshida, N., Kishimoto, T. & Akira, S. Defective adipocyte differentiation in mice lacking the C/EBPβ and/or C/EBPδ gene. *EMBO J.* **16,** 7432–7443 (1997).
26. Omori, Y. *et al.* Mef2d is essential for the maturation and integrity of retinal photoreceptor and bipolar cells. *Genes Cells* **20,** 408–426 (2015).
27. Aoyama, K., Takagi, T., Hirase, A. & Miyazawa, A. STEM tomography for thick biological specimens. *Ultramicroscopy* **109,** 70–80 (2008).
28. Kremer, J. R., Mastronarde, D. N. & McIntosh, J. R. Computer visualization of three-dimensional image data using IMOD. *J. Struct. Biol.* **116,** 71–76 (1996).

© 2016 Macmillan Publishers Limited, part of Springer Nature. All rights reserved.

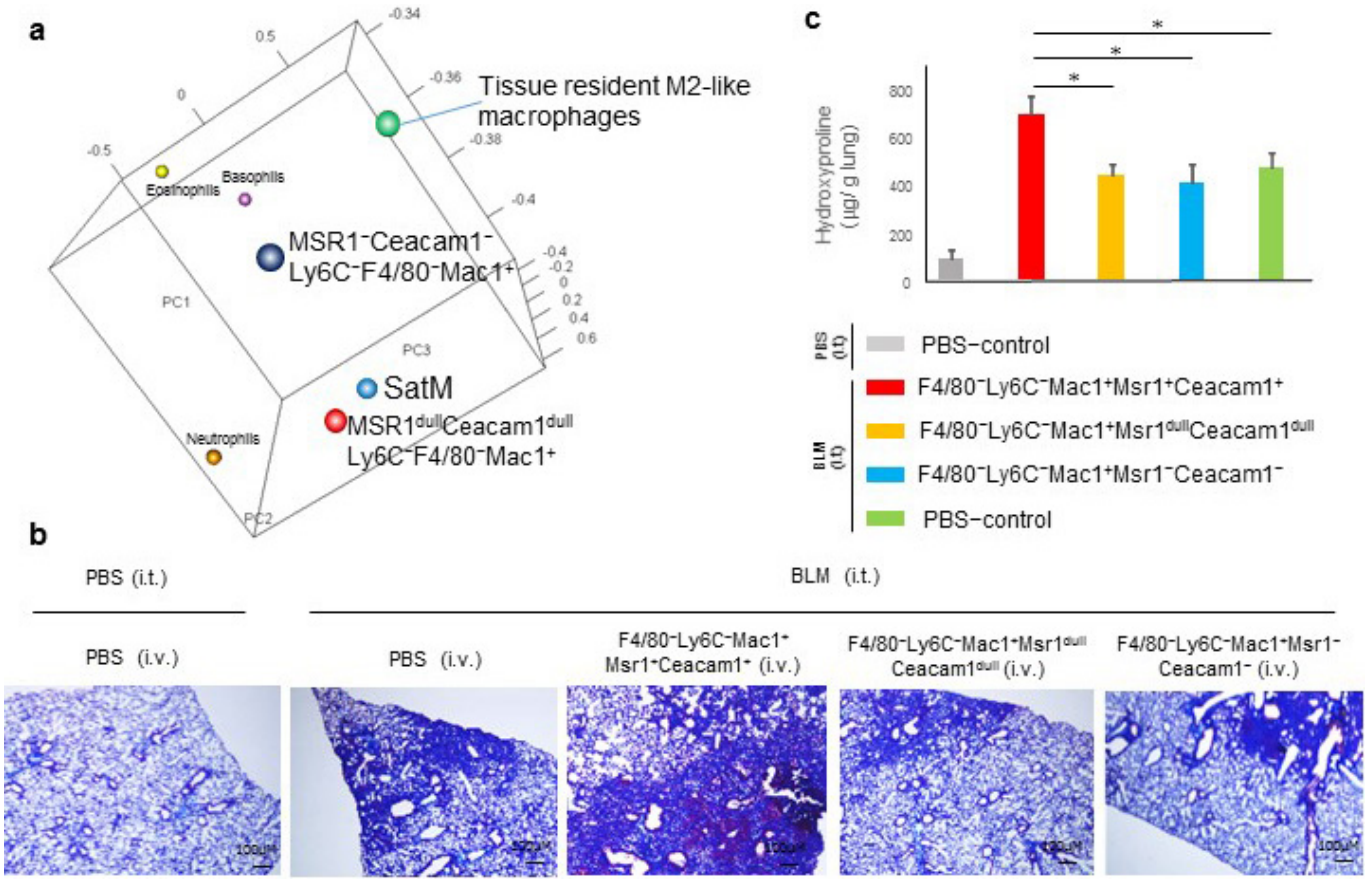

Extended Data Figure 1 | Characterization of various macrophage/ monocytes. a, Indicated cell types were sorted and RNA was collected from them. Each cell type was subjected to microarray analysis. Principal component analysis by using gene expression data was performed. **b**, **c**, Indicated cell types in bone marrow were sorted, and each cell type was adoptively transferred into the wild-type mice, which were administered bleomycin. Images of Azan staining (**b**) and quantity of hydroxyproline are shown (**c**). Similar results were obtained in three independent experiments (**a**–**c**). Scale bars, 100 μm. $*P < 0.05$, $**P < 0.01$.

© 2016 Macmillan Publishers Limited, part of Springer Nature. All rights reserved.

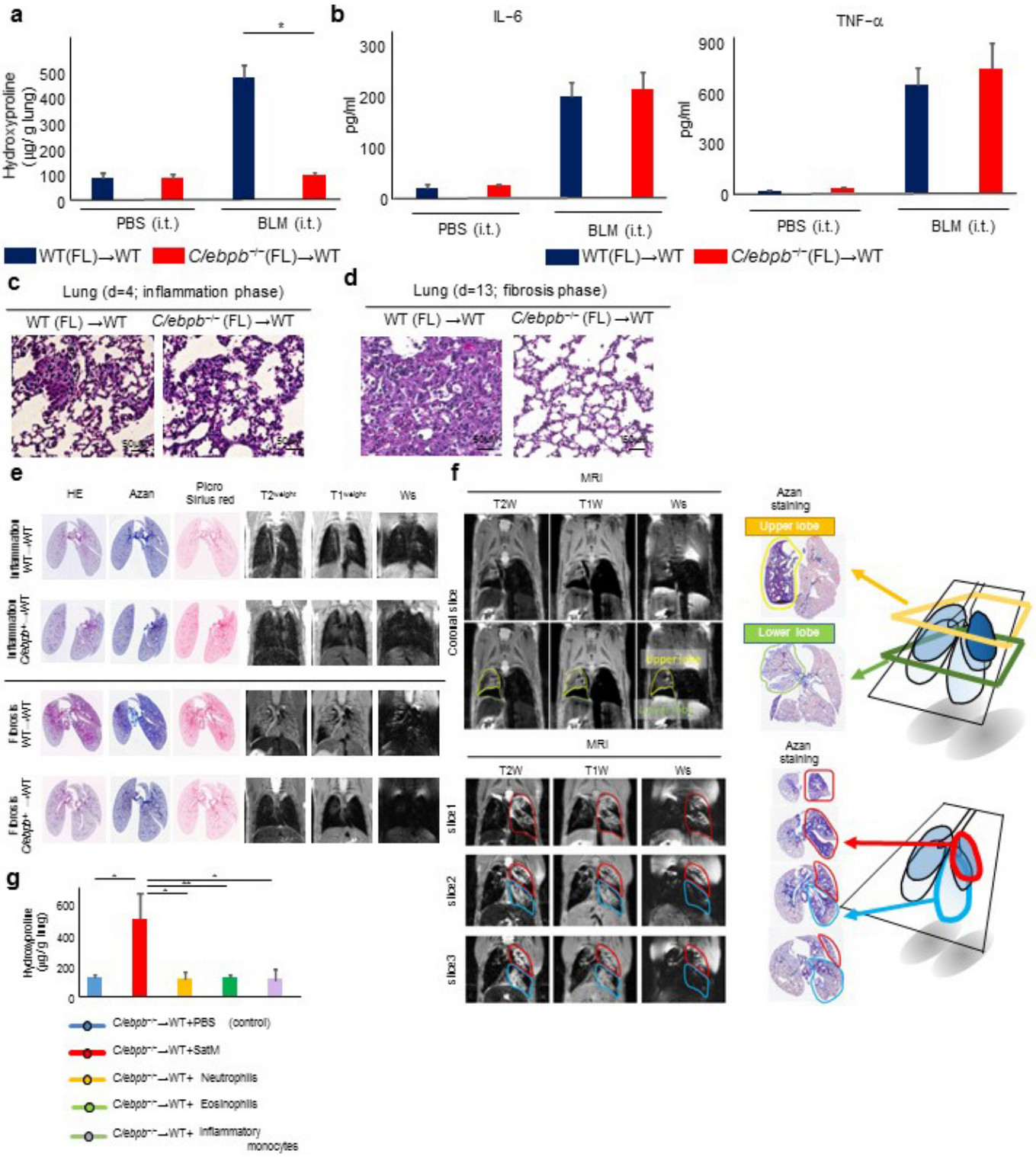

Extended Data Figure 2 | *Cebpb*$^{-/-}$ chimaeras are resistant to the development of fibrosis. **a**, Quantity of hydroxyproline 14 days after bleomycin administration was determined. **b**, Indicated cytokines in the BAL 3 days after bleomycin administration were determined by ELISA. **c**, **d**, Images of H&E staining in the lung tissue 4 days (**c**) and 13 days (**d**) after intratracheal injection with bleomycin. Scale bars, 50 μm. **e**, MRI imaging, H&E, Azan and Sirius red staining of lung. **f**, MRI images of T2 weighted (T2W), T1 weighted (T1W) and water suppression (WS) was shown (left panels). Azan staining of fibrotic lungs and corresponding schematic images of fibrotic region (right panels). **g**, Indicated cell types in bone marrow were sorted, and adoptively transferred into the wild-type mice with bleomycin administration. Quantity of hydroxyproline was shown. Similar results were obtained in three independent experiments (**a**–**g**). $^{*}P < 0.05$, $^{**}P < 0.01$.

© 2016 Macmillan Publishers Limited, part of Springer Nature. All rights reserved.

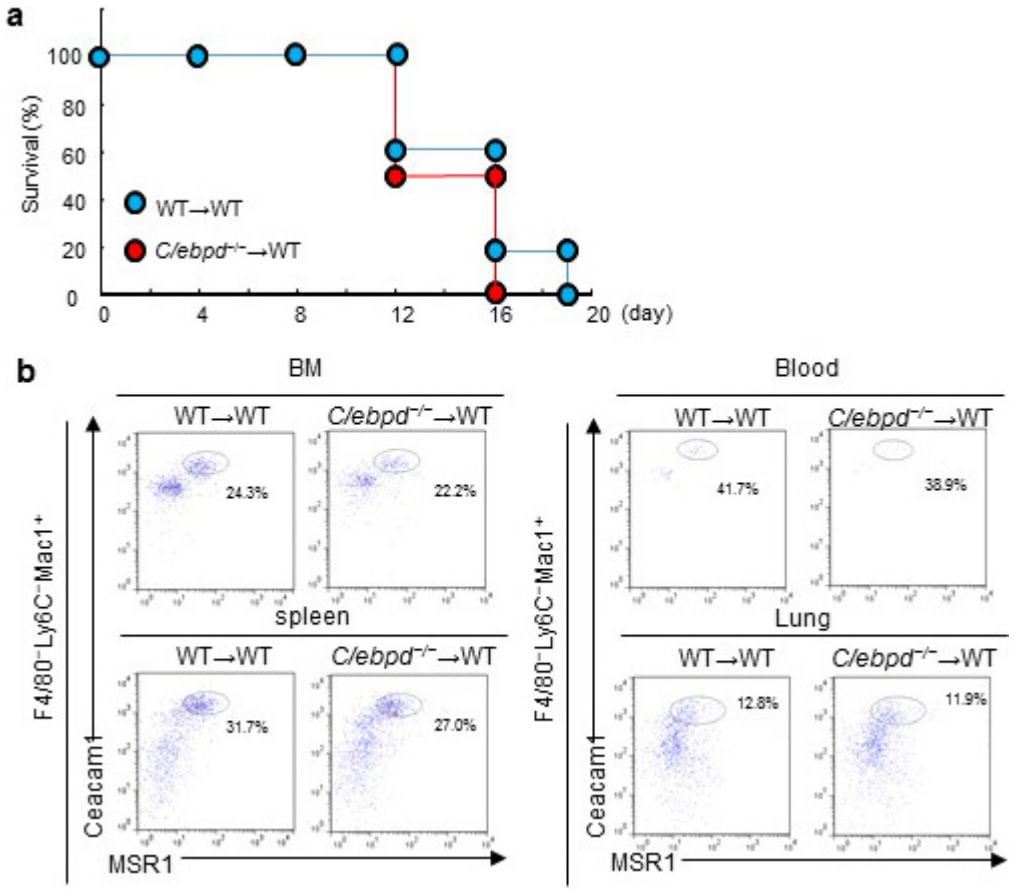

Extended Data Figure 3 | *Cebpd* is dispensable for fibrosis and SatM differentiation. a, The survival rate of chimaeras (at least $n = 5$) inoculated with bleomycin (3 μg per g body weight). Similar results were obtained in three independent experiments. **b**, The proportions of SatM in bone marrow (upper left panel), spleen (bottom left panel), blood (upper right panel) and lung (bottom right panel) were shown. Similar results were obtained in five independent experiments.

© 2016 Macmillan Publishers Limited, part of Springer Nature. All rights reserved.

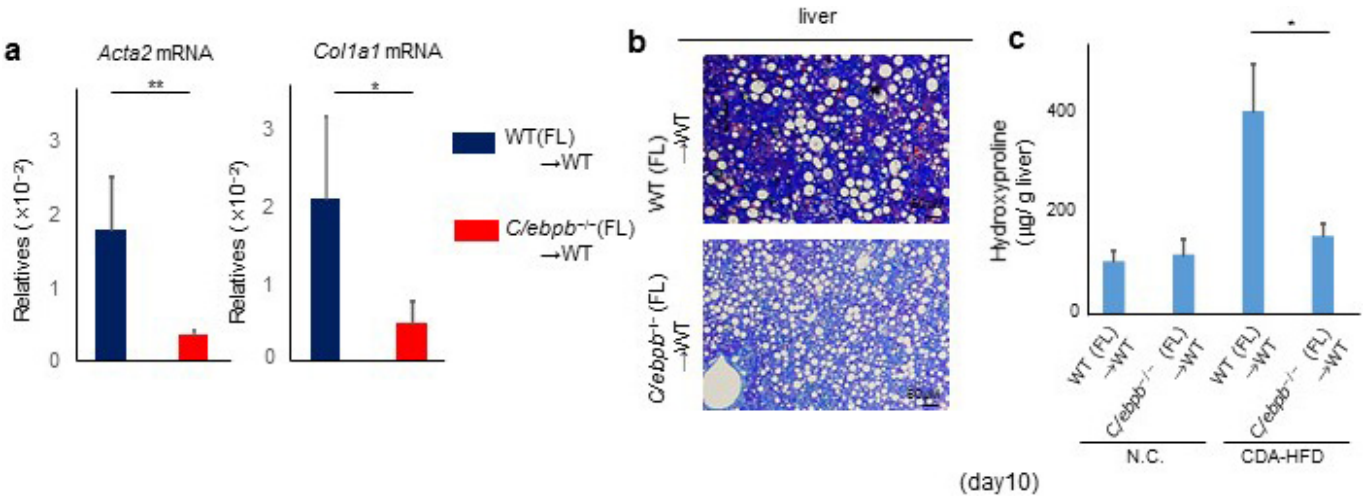

Extended Data Figure 4 | Modified high-fat diet liver fibrosis was repressed in *Cebpb*$^{-/-}$ chimaeras. a, Liver was collected from wild-type and *Cebpb*$^{-/-}$ chimaeric mice fed on CDA-HFD, and indicated mRNA were determined by qPCR. **b**, Images of Azan staining of liver tissue. Scale bar, 50 μm. **c**, Quantity of hydroxyproline was determined. Similar results were obtained in three independent experiments (**a**–**g**). *$P < 0.05$, **$P < 0.01$.

© 2016 Macmillan Publishers Limited, part of Springer Nature. All rights reserved.

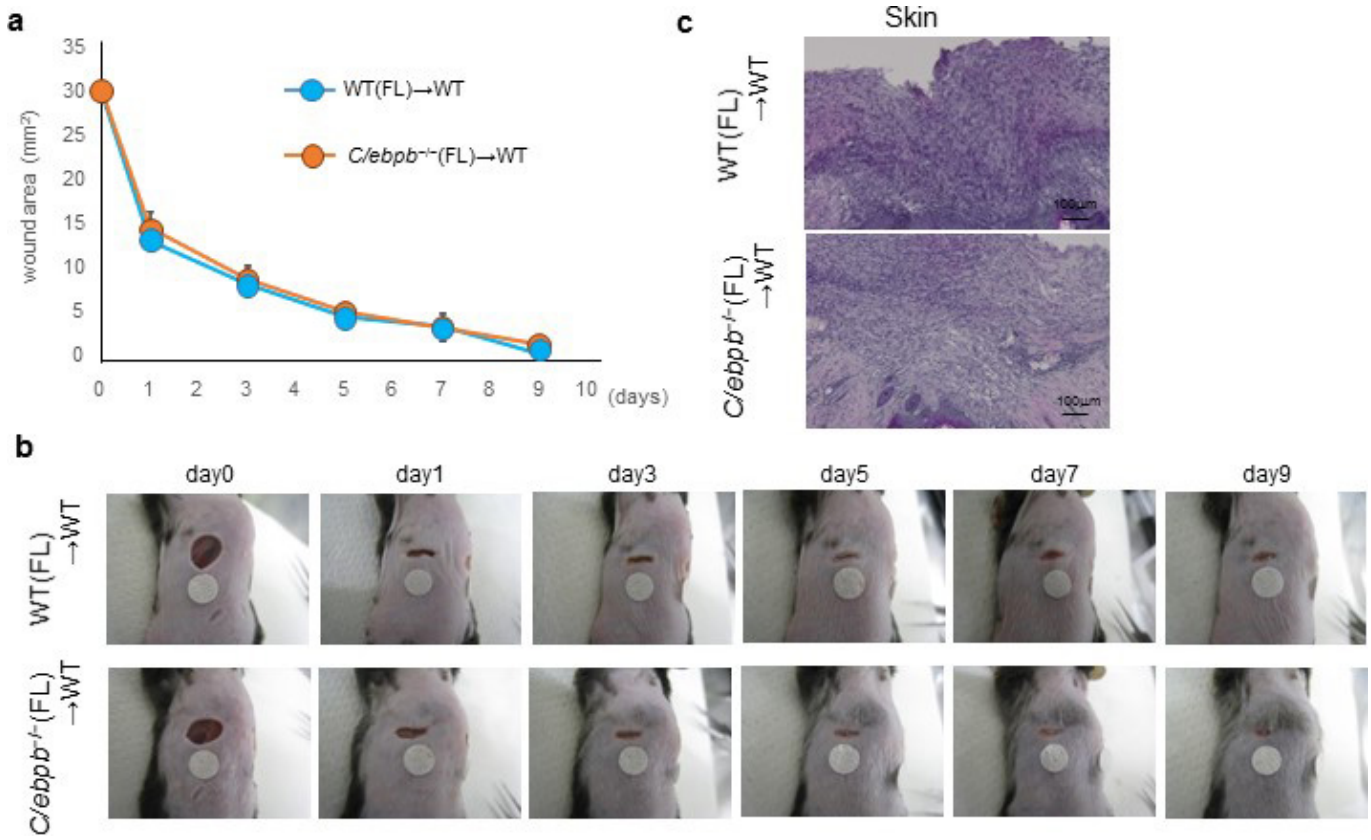

Extended Data Figure 5 | Wound healing progressed normally in *Cebpb*$^{-/-}$ chimaeras. a, **b**, Chimaeric mice with wild-type and *Cebpb*$^{-/-}$ cells (at least $n = 5$) were injured by biopsy (diameter (Φ) = 6 mm). The repair rate of the wound area was monitored. **c**, H&E analysis of skin was performed. Similar results were obtained in three independent experiments.

© 2016 Macmillan Publishers Limited, part of Springer Nature. All rights reserved.

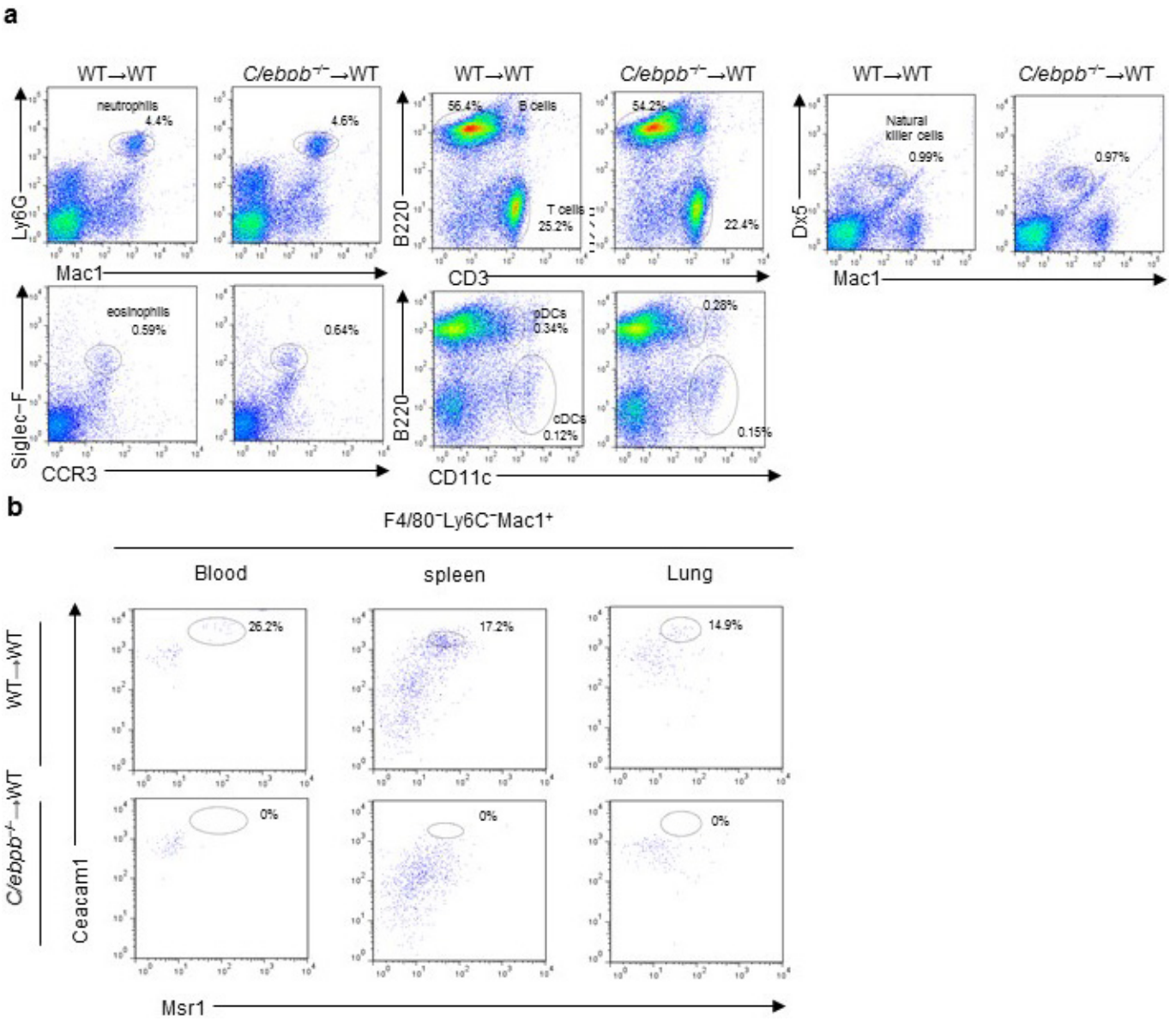

Extended Data Figure 6 | FACS analysis of various immune cells in *Cebpb*$^{-/-}$ chimaeras. a, FACS analysis of spleen. The proportions of neutrophils (upper left), eosinophils (middle left), natural killer cells (bottom left), B cells, T cells (upper right), plasmacytoid dendritic cells (pDC) and conventional dendritic cells (cDC) were shown. **b**, FACS analysis of SatM. The proportions of these cells in blood (left panel), spleen (centre panel) and lung (right panel) were shown. Similar results were obtained in five independent experiments (**a**, **b**).

© 2016 Macmillan Publishers Limited, part of Springer Nature. All rights reserved.

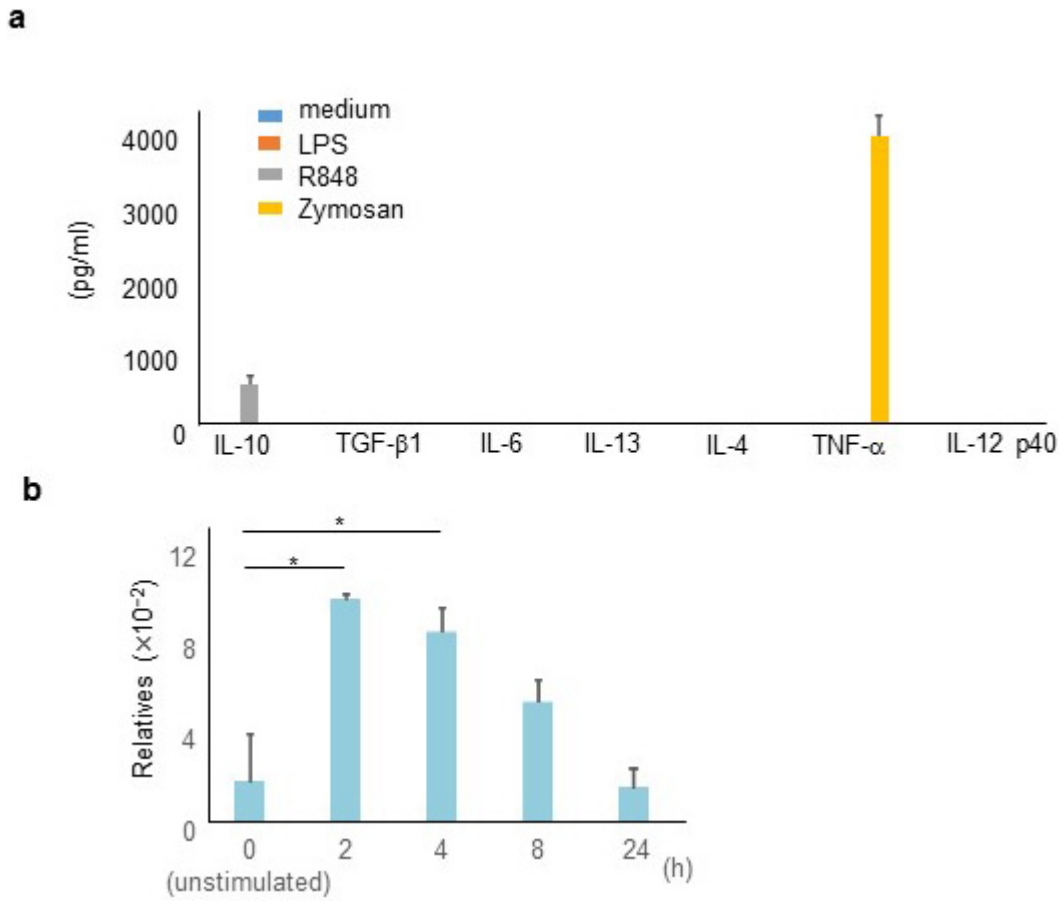

Extended Data Figure 7 | Initiation factor of fibrosis produced from activated SatM. a, Sorted SatM were cultured with Toll-like receptor ligands for 48 h, and concentrations of indicated cytokines were determined by ELISA. **b**, Fibroblasts were cultured with TNF-α for indicated time, and expression level of *Spp1* mRNA was determined by qPCR. Similar results were obtained in three independent experiments (**a**, **b**). $*P < 0.05$, $**P < 0.01$.

© 2016 Macmillan Publishers Limited, part of Springer Nature. All rights reserved.

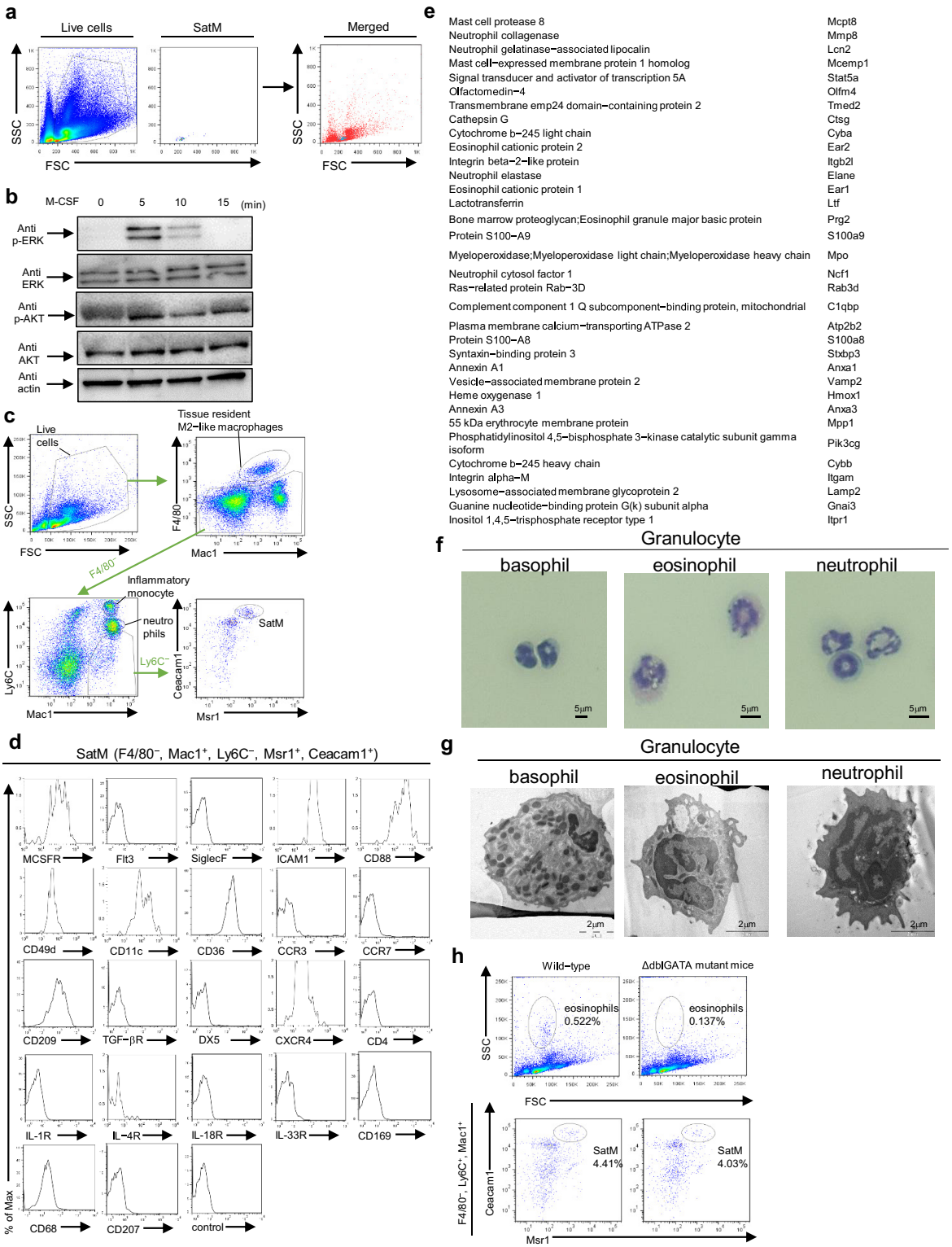

Extended Data Figure 8 | Characterization of SatM. a, The FSC–SSC profiles of whole-cell and SatM in bone marrow (left and centre panels) and merged image (right panel) were shown. Similar results were obtained in three independent experiments. **b**, Expression of phosphorylated (p-) and unphosphorylated Erk and Akt and actin in SatM stimulated with M-CSF (50 ng ml^{-1}). **c**, Flow cytometric analysis of spleen. The proportions of SatM were shown by F4/80^{-}, Mac1^{+}, Ly6C^{-}, Msr1^{+} and Ceacam1^{+}. Similar results were obtained in five independent experiments (**b**, **c**). **d**, The expression level of indicated cell surface molecules of SatM from bone marrow were shown. Similar results were obtained in three independent experiments. **e**, Cell lysates were prepared from SatM in wild-type mice, and were subjected to whole-cell proteomics analysis. Substantially expressed granule proteins were described. **f**, **g**, Sorted Siglec-F^{+}CCR3^{+}CD4^{-} population, Ly6G^{+}Mac1^{+} population and DX5^{+}FcεRI^{+}c-kit^{-}CD3^{-}CD19^{-} population were stained with Diff-Quick after cytospin centrifugation and were photographed (**f**) and investigated by TEM (**g**). Scale bars were shown in indicated images. Similar results were obtained in three independent experiments (**f**, **g**). **h**, Flow cytometric analysis of spleen obtained from wild-type and ΔdblGATA mutant mice. The proportions of eosinophils (upper panel) and SatM (bottom panel) were shown. Similar results were obtained in five independent experiments.

© 2016 Macmillan Publishers Limited, part of Springer Nature. All rights reserved.

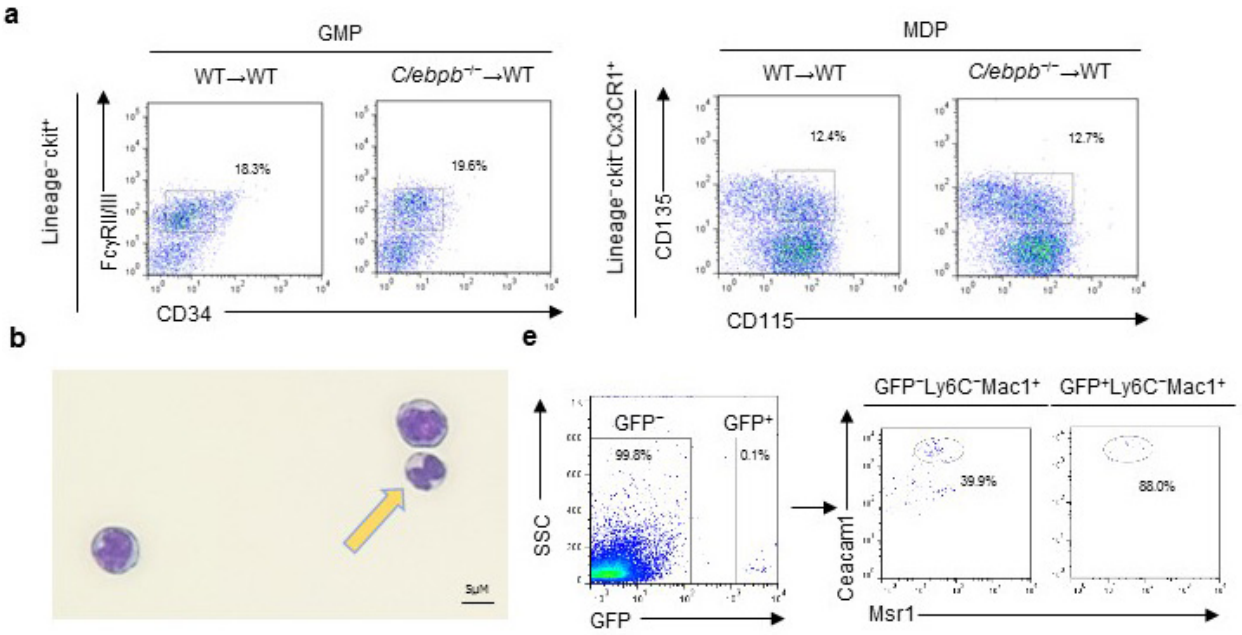

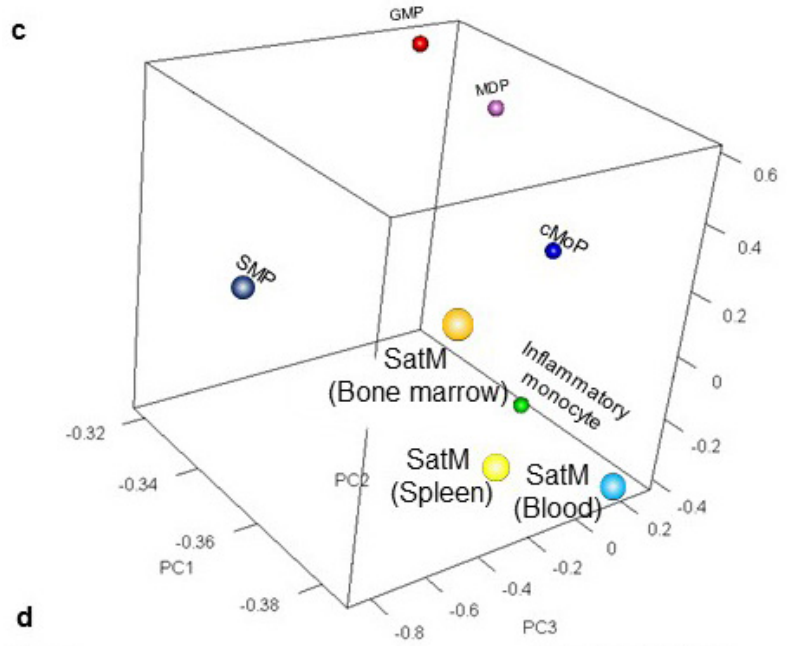

d

Cluster	Transcriptional factors																
I	Elf1	Fli1	Etv3	Ets2	Elk3	Elk4	Etv6	Gatad1	Gatad2b	Cebpz	Klf3	Klf4	Mef2a	Runx1	Nfkb1	Nfkbiz	Nfatc1
	Nfatc3	Stat1	Stat5a	Stat5b	Stat6	Smad3	Smad4	Notch1	Foxk1	Foxk2	Foxn3	Foxo4	Mcm4	Mcm7	Nr2c2	Nr2f6	Nr3c1
II	Elf2	Elf4	Gabpa	Gabpb1	Sfpi1	Cebpg	Cebpd	Klf9	Klf16	Irf1	Irf3	Irf9	Lmo4	Lyl1	Mef2d	Mef2b	Mafg
	Runx3	Jdp2	Rela	Nfkbid	Creb1	Nfat5	Stat4	Smad2	Foxj3	Dnmt3a	Dnmt3b	Mcm2	Mcm3	Mcm5	Mcm6	Mcm9	Rxrb
III	Erf	Spic	Elk1	Klf2	Ikzf5	Irf7	Bach2	Per1	Maf	Mafb	Tcf7l2	Nfkb2	Rel	Nfkbib	Nfkbil1	Creb3l2	Stat2
	Smad5	Smad7	Rarg	Pparg	Nr1h2	Rxra	Nr2c1	Esrra	Nr4a2								
IV	Ets1	Cebpb	Egr1	Klf7	Klf11	Ikzf3	Irf2bpl	Mafk	Nfkbie	Nfatc2	Stat3	Foxj2	Foxo1	Nr4a1			
V	Etv5	Spib	Lmo1	Sox4	Gfi1	Per3	Myc	Foxm1	Foxp4	Trdmt1	Mcm8	Mcm10	Vdr	Esr1			
VI	Gata1	Gata2	Egr2	Egr3	Klf5	Ikzf2	Tal1	Dach1	Gfi1b	Junb	Crem	Foxd2	Foxq1	Rora			
VII	Gatad2a	Cebpa	Klf6	Klf10	Klf13	Ikzf1	Irf2	Irf2bp2	Lmo2	Myb	Bach1	Runx2	Fos	Jun			
	Jund	Nfkbia	Atf4	Creb3	Smad1	Notch2	Foxn2	Foxo3	Foxp1	Dnmt1							
VIII	Irf4	Irf5	Irf8	Mef2c	Mitf	Nr1d2											

Extended Data Figure 9 | Characterization of various progenitors. **a**, The proportion of GMPs (left panel) and MDPs (right panel) were shown. Similar results were obtained in three independent experiments. **b**, Sorted Ly6C$^-$FcεRI$^+$ GMP population were stained with Diff-Quick after cytospin centrifugation and were photographed. Similar results were obtained in five independent experiments. **c**, Principal component analysis by using gene expression of indicated cells was performed. **d**, SatM, inflammatory monocytes, SMPs, cMoPs, MDPs and GMPs were sorted and subjected to microarray analysis. Data on transcription factor genes were partitioned by *k*-means clustering using the threshold $k = 8$. Clustered molecules are shown. **e**, Sorted GFP$^+$Lin$^-$c-kit$^-$ C5aR$^+$CD115$^+$FcεRI$^+$Ly6C$^-$ populations were transferred into wild-type mice, and then analysed by FACS. Similar results were obtained in three independent experiments.

© 2016 Macmillan Publishers Limited, part of Springer Nature. All rights reserved.

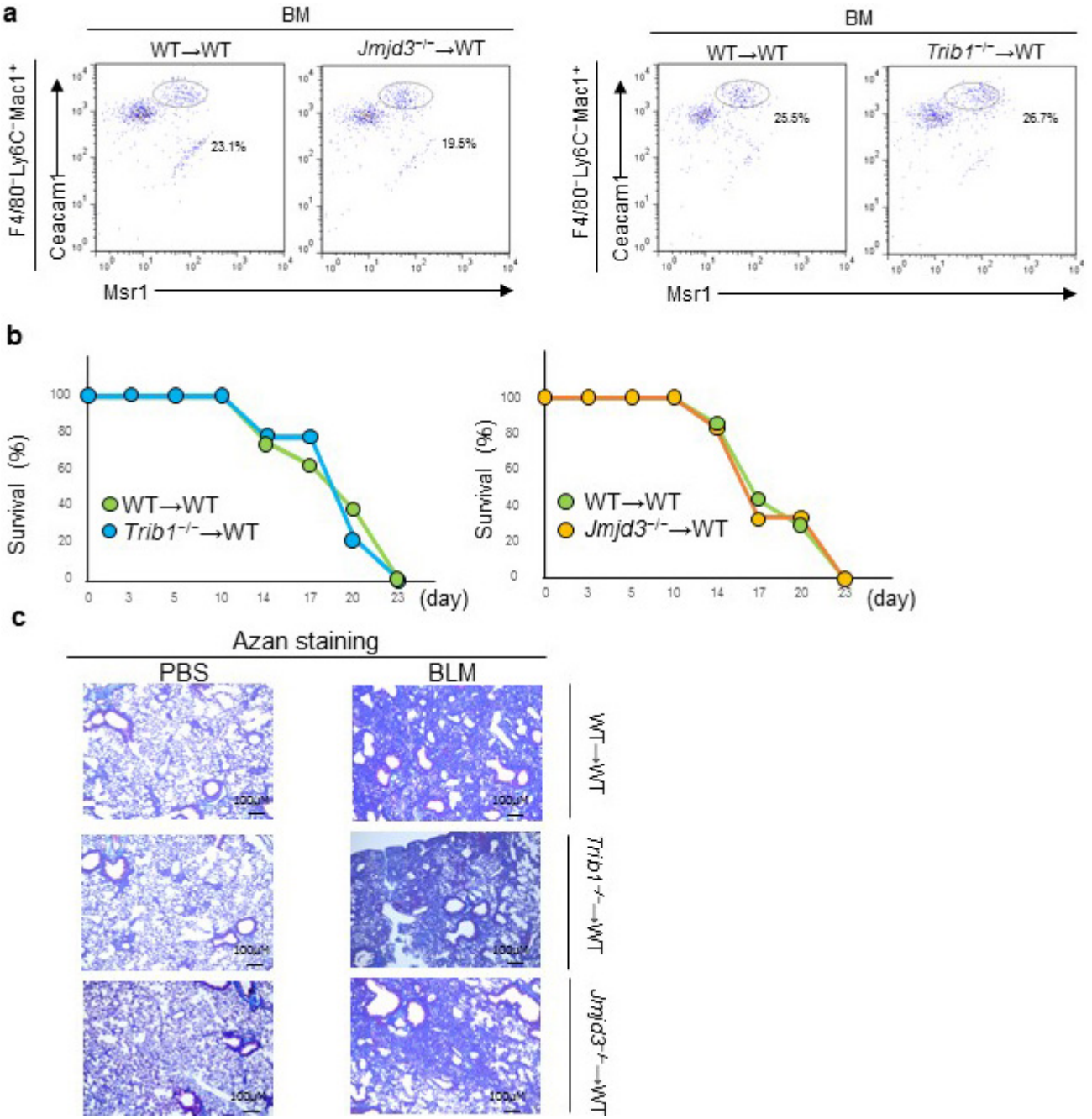

Extended Data Figure 10 | Macrophages regulated by Jmjd3 and Trib1 were dispensable for the development of fibrosis. a, The proportion of SatM in *Jmjd3*$^{-/-}$ (left panel) and *Trib1*$^{-/-}$ (right panel) were shown. Similar results were obtained in five independent experiments. **b**, **c**, Chimaeric mice with wild-type, *Jmjd3*$^{-/-}$ or *Trib1*$^{-/-}$ haematopoietic cells (at least $n = 5$) were intratracheally inoculated with bleomycin (3 μg per g body weight). The survival rate of mice was monitored (**b**). Images of Azan staining for collagen fibres in the lung tissue of wild-type, *Jmjd3*$^{-/-}$ and *Trib1*$^{-/-}$ bone marrow chimaeric mice (**c**). Similar results were obtained in three independent experiments.

© 2016 Macmillan Publishers Limited, part of Springer Nature. All rights reserved.